Contents lists available at: http://qu.edu.iq

Al-Qadisiyah Journal for Engineering Sciences

Journal homepage: https://qjes.qu.edu.iq

Research Paper

# Flow and heat transfer augmentation using helical coiled wire of different cross-sections

***Murtadha A. Hanoon*** [1,2], ***Mohsen H. Fagr*** [1], ***and Kamaal S. Mekki*** [1]

[1] *Department of Mechanical Engineering, College of Engineering, University of Thi-Qar, ThiQar, 64001, Iraq.*
[2] *Thi-Qar Oil Company (TOC), Oil Compound, Nassiriyah, Iraq.*

ARTICLE INFO

*Article history*:
Received 08 January 2024
Received in revised form 14 June 2024
Accepted 15 May 2025

*keyword*:
Coiled-Coil wire
Fluid dynamics modeling
Heat exchanger design
Improvement of heat transfer
Tube insert configurations
Helical wire

ABSTRACT

In this numerical investigation, the effectiveness of utilizing advanced helical coiled wires (HCWs) as a tube insert for heat transfer and turbulence enhancement under turbulent flow conditions (Reynolds numbers: 3000-11000) was examined. HCW followed a helical guide path instead of a straight one in a typical coiled wire case, resulting in increased flow complexity. Circular and equilateral triangular wires, maintaining equal cross-sectional areas, were tested, with pitch ratios (P/D) being 1, 1.5, and 2. Simulation was performed using ANSYS Fluent 22, and the working fluid considered throughout the study was air. Results indicated increased Nusselt number ($Nu$) and friction factor ($f$) compared to a plain tube. The thermal performance factor was found to have an inverse relationship with both pitch ratio and Reynolds number separately. The study reported that the circular insert at $(P/D) = 1$ and $Re = 3000$ exhibited the maximum thermal performance factor of 1.379, while the highest enhancement ratio for Nusselt number of 4.14 was recorded in the case of the triangular insert at the same Reynolds number. Additionally, the maximum friction factor increases up to 40.4 at the Re=11000 of the triangular model.



## 1. Introduction

Heat transfer is an essential process that holds a crucial role in diverse industrial, engineering, and scientific applications. It refers to the process of thermal energy transfer from one region to another due to a temperature difference. Understanding and optimizing heat transfer mechanisms are essential for designing efficient systems and devices. The three primary forms of heat transfer are radiation, convection, and conduction. Although each mode has importance, convection is especially noteworthy because of its broad applicability and influence on real-world situations. This mode of heat transfer is of paramount importance in numerous applications, such as industrial cooling processes [1], thermal management in electronic devices [2], aerospace propulsion systems [3], and even natural phenomena like weather patterns and ocean currents [4]. The efficiency of convective heat transfer directly influences the performance and energy consumption of these systems. Heat exchangers (HEs) are devices that transfer heat between two or more fluids. The heat transfer occurs through the process of convection in each fluid and conduction through the wall separating the two fluids. The efficacy of these heat exchangers plays a pivotal role in determining the overall efficiency of the associated systems. Enhancing the performance of HEs offers manifold advantages, including compact design, cost-effectiveness in both manufacturing and operation, and energy conservation. Consequently, investigating methods to augment heat transfer has garnered significant attention among researchers [5]. Incorporating turbulence flow generators stands out as an effective approach for enhancing composite velocity and optimizing heat transfer within heat exchanger tubes. These generators serve to disrupt the thermal boundary layer and amplify tangential and radial turbulent fluctuations [6]. Among the various turbulence flow generators, Coiled Wires (CWs) stand out as an effective means to induce swirl or turbulence near the tube wall, which leads to more efficient fluid mixing between the near-wall and core regions, resulting in an enhanced heat transfer process. The unique geometric configuration of helical wire inserts generates vortices, swirls, and secondary flows within the fluid trajectory as it passes over the inserts. This phenomenon facilitates intensified fluid mixing and heightened interaction between the fluid and tube walls, thereby leading to an elevated heat transfer coefficient. The literature delved into the significance of coiled wire inserts as a crucial passive heat transfer enhancement technique, garnering attention in thermal engineering research over recent decades. Researchers aim to optimize designs, facilitating the development of more efficient and compact heat exchanger systems. García et al., 2012 [7], compared the thermal-hydraulic behavior of corrugated tubes, dimpled tubes, and wire coils. Wire coils were identified as the optimal choice for Reynolds numbers between 200 and 2000 in heat exchangers. Chang et al., 2015 [8] investigated the impacts of grooved square wire coils, illustrating enhancements in both heat transfer and thermal performance in comparison to tubes with smooth-coil tubes. San et al., 2015 [9] conducted an experimental analysis on thermo-hydraulic characteristics within a system incorporating a coiled wire insert, highlighting the significance of the wire diameter to tube diameter ratio and the coil pitch to tube inner diameter ratio. Sharafeldeen et al., 2017 [10] studied the effect of wire coil insertion in a smooth tube under constant heat flux and variable Reynolds numbers, revealing significant increases in heat transfer and friction factor. Du et al., 2018 [11] experimentally studied the effect of regularly spaced wire coils with a conical shape inside traverse corrugated tubes, noting increased friction factor and heat transfer. Zimparov et al., 2022 [12] explored the effect of the pitch of the inserted coiled wire on the heat exchanger performance experimentally, identifying the greatest benefits with a pitch of p/e = 10.0. The impact of a square cross-sectional wire inserted into a circular plain pipe on the thermo-hydraulic characteristics of the flow field was studied numerically by Hinge et al., 2019 [13].

*Corresponding Author.
E-mail address: murtadha.a.h@utq.edu.iq ; Tel: (+964) 781-200 9292 (Murtadha Hanoon)

https://doi.org/10.30772/qjes.2024.145936.1081
2411-7773 

**Nomenclature**

| | | | |
|---|---|---|---|
| $a$ | Triangle side length $(mm)$ | *Greek symbols* | |
| $C_p$ | Specific heat $(J\ kg^{-1}K^{-1})$ | $\mu$ | dynamic viscosity $(kg\ m^{-1}s^{-1})$ |
| $D$ | Tube diameter $(mm)$ | $\rho$ | density $(kg\ m^{-3})$ |
| $e$ | Wire diameter $(mm)$ | *Subscripts* | |
| $f$ | Darcy friction factor | $p$ | Plain tube |
| $f_p$ | Darcy friction factor for plain tube | $f$ | Fluid |
| $k$ | thermal conductivity $(W\ m^{-1}K^{-1})$ | *Abbreviations* | |
| $L$ | Tube length $(mm)$ | CHCW | Circular helical coiled wire |
| $Nu$ | Average Nusselt number | CHCW-NT | Circular helical coiled wire without taper |
| $Nu_p$ | Average Nusselt number for plain tube | CHCW-TD | Decreased Tapered circular helical coiled wire |
| $P$ | Guide path pitch length $(mm)$ | CW | Coiled wire |
| $p$ | Coiled wire pitch length $(mm)$ | HCW | Helical coiled wire |
| $P_r$ | Prandtl number | HCW-T | Tapered helical coiled wire |
| $r$ | Coiled wire centreline radius $(mm)$ | HCW-TD | Decrease tapered helical coiled wire |
| $R1$ | Large base radius $(mm)$ | HE | Heat exchanger |
| $R2$ | Small base radius $(mm)$ | PT | Plain tube |
| $Re$ | Reynolds number | THCW | Triangular helical coiled wire |
| $S$ | Space between the wire and the tube surface $(mm)$ | THCW-NT | Triangular helical coiled wire without taper |
| $T$ | Temperature $(K)$ | THCW-TD | Decreased tapered triangular helical coiled wire |
| $u, v, w$ | Mean velocity components $(m/s)$ | TR | Taper ratio |

The findings indicated that rising turbulence and velocity levels led to rising heat transfer coefficients. Yu, Chulin, et al., 2020 [14] investigated wire coils with different cross-sectional shapes in a twisted oval tube through numerical simulation, revealing enhanced heat transfer and increased pump consumption. Sharifi, et al., 2020 [15] investigated the application of artificial neural networks and genetic algorithms to anticipate the values of heat transfer and pressure drop of tubes with wire coils under non-isothermal conditions. Yang et al., 2021 [16] investigated wire coil inserts in annular channels for molten salt heat exchangers, indicating significant heat transfer enhancement with proposed correlations for friction factor and Nusselt number. Göksu et al., 2021 [17] employed numerical simulations to study the impact of various wire coil geometries and pitch ratios on heat transfer and pressure drop in a square duct. Wei Dang and Liang-Bi Wang, 2021 [18] explored a new twined coil insert to enhance heat transfer in a tube through numerical analysis and experiments, presenting correlations for Nusselt number and friction factor. A numerical investigation was conducted by Aldawi, Fayez., 2022 [19] to analyse the thermal and frictional properties of a flat coil tube with spring inserts, emphasizing the enhanced heat transfer performance while taking into account the pressure drop. A. García et al., 2023 [20] explored the efficacy of wire-coils in enhancing heat transfer at low Reynolds numbers. A novel methodology based on TSP (Transition Shape Parameter) predicted friction coefficient evolution and extended transitional flow regions. Results from harp-type solar collectors indicated that wire-coil geometries with lower ReCL values significantly enhanced heat transfer, offering potential absorber temperature reductions of up to 15%. The findings underscored the importance of selecting wire-coil geometries that aligned with application-specific Reynolds number ranges for optimal thermal performance and minimal pressure losses. Rajan Kumar et al., 2023 [21] investigated the impact of coiled spring turbulators on heat transfer and pressure drop in a triple tube heat exchanger using water and CuOwater (0.8%vol/vol) as working fluids. Results showed that lower-pitched inserts combined with CuO nanofluid achieved the highest heat transfer enhancement, especially in counter flow arrangements. Notably, at $Re = 4000$, the heat transfer coefficient for the lower pitch spring insert with CuO nanofluid was 144.74% higher than that of the plain tube with water. In counter flow, the Nusselt number augmentation for the triple tube with lower spring pitch and CuO nanofluid was 63.33% higher compared to the plain triple tube with water. The maximum thermal performance value was observed in the plain tube with CuO nanofluid, reaching 1.04 at $Re = 4000$. Furthermore, thermal performance enhancement was greater in counter flow arrangements compared to parallel flow configurations. Turbulent flow within a parabolic solar collector tube equipped with two spring insert samples of varying pitch ratios ($P/D = 0.22,\ 0.44$) and a specific cross-section was studied and simulated by Peng Yin et al., 2023 [22], $Cu–Fe3O4$/Water hybrid nanofluid with volume fractions of $\phi = 1\%, 3\%,$ and$5\%$ was analysed across Reynolds numbers of 7000, 9000, and 11000. Results indicated that decreasing the pitch ratio led to increased Nusselt number and solar collector efficiency, with maximum efficiency observed at $P/D = 0.22$ ($Re = 7000$, $\phi = 1\%$). The Field Synergy Principle highlighted the positive impact of the spring insert on heat transfer rate and solar collector efficiency. Lower pitch ratios were recommended for optimal solar collector efficiency. Orhan Keklikcioglu and Veysel Ozceyhan, 2022 [23] analysed the effects of using convergent, convergent-divergent, and divergent conical wire coils in ethylene glycol and water mixture flow regions on heat transfer augmentation. Three different volumetric ratios of ethylene glycol and water were investigated, along with two pitch ratios for the wire coils. Results showed that conical wire coils enhanced heat transfer rate and increased fluid friction, with the highest Nusselt number achieved with a divergent coil at a (40:60) volumetric ratio. New correlations were proposed to predict Nusselt number and friction factor, suggesting potential for improving thermohydraulic performance in engineering applications. Key conclusions included the effectiveness of ethylene glycol dispersion in water for varying temperature conditions and the significant impact of pitch ratio on heat transfer and pressure drop. The study underscored the potential of conical wire coils as an economical solution for enhancing heat transfer in thermal systems. In summary, the literature review synthesized findings from both experimental and numerical studies, providing a comprehensive understanding of the effectiveness of wire coil inserts in enhancing heat transfer. It identified gaps in research, such as the absence of studies on helical coiled wire with circular or triangular cross-sections. The present investigation endeavours to address a portion of the existing knowledge gap in this field.

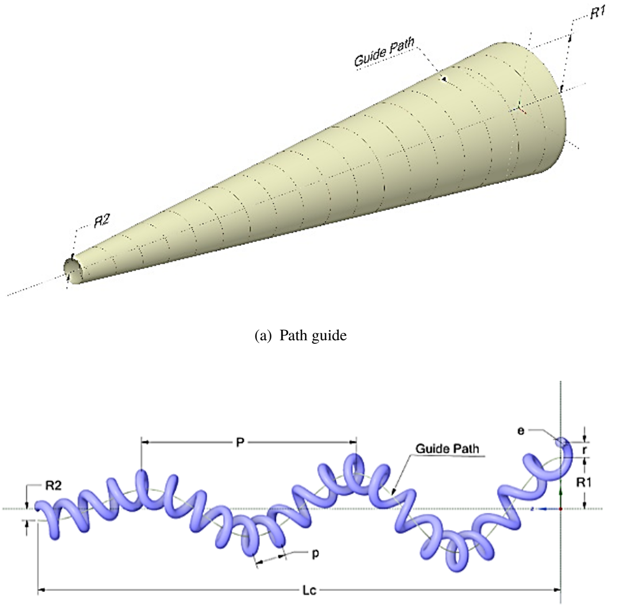


(a) Path guide

(b) Wire geometry

**Figure 1.** ANSYS design modeler that include (a) Conical representative of the guide path; (b) Tapered helical coiled wire geometry parameters.

## 2. Modeling approach and methodology

### 2.1 . Physical modeling

The present study proposed a helical coiled wire (HCW) geometry as an inserted device. It offers a higher level of complexity and accordingly a higher level of turbulence compared to the typical helical wire arrangement. This geometry consists of a helical wire that is coiled around a secondary helical path, which serves as a virtual guide path.

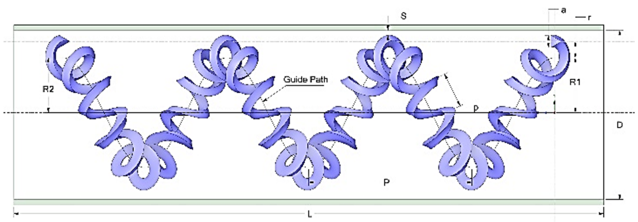


**Figure** 2. Equilateral triangular helical coiled wire fitted into a tube.

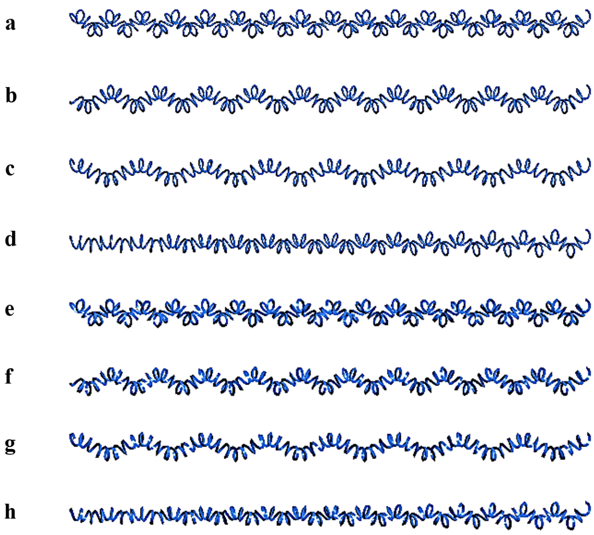


**Figure** 3. Helical coiled wires of different configurations; a) CHCW-NT_1_7_10; b) CHCW-NT_1.5_7_10; c) CHCW-NT_2_7_10; d) CHCW-TD_1_7_10; e) THCW-NT_1_7_10; f) THCW-NT_1.5_7_10; g) THCW-NT_2_7_10; and h) THCW-TD_1_7_10.

**Table** 1. Names and dimensions of the models.

| No. | Name | $p/D$ | $R1,\ mm$ | $r, mm$ | $p, mm$ |
|---|---|---|---|---|---|
| 1 | $CHCW-NT\_1\_7\_10$ | 1.0 | 7 | 6.00 | 10 |
| 2 | $CHCW-NT\_1.5\_7\_10$ | 1.5 | 7 | 6.00 | 10 |
| 3 | $CHCW-NT\_2\_7\_10$ | 2.0 | 7 | 6.00 | 10 |
| 4 | $CHCW-TD\_1\_7\_10$ | 1.0 | 7 | 6.00 | 10 |
| 5 | $THCW-NT\_1\_7\_10$ | 1.0 | 7 | 5.65 | 10 |
| 6 | $THCW-NT\_1.5\_7\_10$ | 1.5 | 7 | 5.65 | 10 |
| 7 | $THCW-NT\_2\_7\_10$ | 2.0 | 7 | 5.65 | 10 |
| 8 | $THCW-TD\_1\_7\_10$ | 1.0 | 7 | 5.65 | 10 |

The guide path plays an essential role in defining the helical coiled wire and tapered helical coiled wire (HCW-T) geometries, in turn, it can be defined by the helical line that tangents at all points to the surface of a hypothetical cylinder with base radius is R1 in the case of HCW, or in the more general case HCW-T, it is the helical line tangents at all points to the surface of a hypothetical truncated cone with large base and small base radii are R1 and R2, respectively. Figure 1 depicts a schematic diagram for a guide path contained in a truncated cone and tapered helical coiled wire geometry parameters. HCW-T can be described by a number of dimensions, which are; guide path pitch (P), coiled wire pitch (p), large base radius (R1), small base radius (R2), coiled wire centerline radius (r), and wire diameter (e). The proposed HCW-T geometry stands as a more encompassing form of the typical helical wire arrangement, by allowing the pitch value (P) of the guide path to tend towards infinity, and $R2 = R1 = 0$, the geometry seamlessly transformed into typical helical wire configuration without tapering. One type of HCW-T was used in this study, that is tapered decrease helical coiled wire (HCW-TD), formulated when the large base radius R1 is located in the flow inlet region. In addition to the helical coiled wire with a circular cross-section (CHCW) with a wire diameter of ($e = 2\ mm$), the present study proposed numerous models of the helical coiled wires with an equilateral triangular cross-section (THCW) with a triangle side length of ($a = 2.7\ mm$), which results in an almost equal cross-sectional area for both shapes. Figure 2 depicts a schematic diagram for an equilateral triangular helical coiled wire fitted into a tube of length (L), inner diameter (D), and the clearance between the wire and the inner surface of the tube (S). The studied cases were simulated in the physical model with the assistance of ANSYS DesignModeler, while ANSYS SpaceClaim was used for some illustrative graphics schemes. The circular tube was a stationary, horizontal installation, 30 $mm$ in diameter and 500 $mm$ in length. The clearance ($S = 1\ mm$) for all models. In the present study, the dimensionless quantity defined as pitch ratio (P/D) emerges as a critical factor shaping the geometry of the tested models. This parameter defines the relationship between the pitch length (P) of the guide path and the tube diameter (D). Three pitch ratios of 1, 1.5, and 2 were used, resulting from the pitches (P) values of 30 $mm$, 45 $mm$, and 60 $mm$. Another important non-dimensional quantity that is described tapered helical coiled wire geometry in the present study is the taper ratio ($TR = R2/R1$), defined as the ratio of the small base radius (R2) to the large base radius (R1), all tested tapered models have the same tapered ratio of ($TR = 0.21$). The large base radius (R1) and the coiled wire pitch (p) are maintained constant at 7 $mm$ and 10 $mm$, respectively. The models were named according to the following pattern **XXXX-XX_P/D_R1_p**. Where the field (XXXX-XX) denotes the model's abbreviation. The impacts of helical coiled wire inserts with circular and equilateral triangular cross-sections were examined in this study using eight different models. These models were designed to explore various configurations with different pitch ratios (P/D), Table 1. provides the names and dimensions of these models. The different HCWs configurations that were studied in the current investigation are shown in Fig. 3. The tool of choice for executing simulations and computations in this study was ANSYS-22R1.

### 2.2 . Governing equations and boundary conditions

In the computational simulations carried out in the present investigation, various flow assumptions have been taken into account, with the working fluid being air, the flow is assumed to be three-dimensional, steady-state, turbulent, and incompressible. Additionally, the neglect of body forces, thermal radiation, and natural convection is incorporated into the simulation model. The assumed thermo-physical characteristics of the fluid remain constant with temperature, specified as ($\rho = 1.225\ kg/m^3$, $\mu = 1.789 \times 10^{-5}\ kg/(ms)$, $C_p = 1006.43\ J/kgK$, and $K = 0.0242\ W/mK$). The thickness of the tube wall is considered negligibly small. The concise expressions for the governing equations, represented by Eq. 1 up to Eq. 5, can be generally formulated as follows:

The equation of continuity, Eq. 1:

$$\frac{\partial u}{\partial x} + \frac{\partial v}{\partial y} + \frac{\partial w}{\partial z} = 0 \tag{1}$$

The equation of momentum along the X-axis Eq. 2:

$$\rho\left(u\frac{\partial u}{\partial x} + v\frac{\partial u}{\partial y} + w\frac{\partial u}{\partial z}\right) = -\frac{\partial p}{\partial x} + \mu\left(\frac{\partial^2 u}{\partial x^2} + \frac{\partial^2 u}{\partial y^2} + \frac{\partial^2 u}{\partial z^2}\right) \tag{2}$$

The equation of momentum along the Y-axis Eq. 3:

$$\rho\left(u\frac{\partial v}{\partial x} + v\frac{\partial v}{\partial y} + w\frac{\partial v}{\partial z}\right) = -\frac{\partial p}{\partial y} + \mu\left(\frac{\partial^2 v}{\partial x^2} + \frac{\partial^2 v}{\partial y^2} + \frac{\partial^2 v}{\partial z^2}\right) \tag{3}$$

The equation of momentum along the z-axis Eq. 4:

$$\rho\left(u\frac{\partial w}{\partial x} + v\frac{\partial w}{\partial y} + w\frac{\partial w}{\partial z}\right) = -\frac{\partial p}{\partial z} + \mu\left(\frac{\partial^2 w}{\partial x^2} + \frac{\partial^2 w}{\partial y^2} + \frac{\partial^2 w}{\partial z^2}\right) \tag{4}$$

The equation of energy conservation Eq. 5:

$$\rho C_p\left(u\frac{\partial T}{\partial x} + v\frac{\partial T}{\partial y} + w\frac{\partial T}{\partial z}\right) = K_f\left(\frac{\partial^2 T}{\partial x^2} + \frac{\partial^2 T}{\partial y^2} + \frac{\partial^2 T}{\partial z^2}\right) \tag{5}$$

The boundary conditions used for solving the governing equations were for tube; stationary wall boundary condition, tube wall was exposed to a constant heat flux of (1500 $W/m^2$), constant temperature at the inlet of (298 K), uniform velocity at the inlet of the value corresponding to Reynold numbers of 3000, 5000, 7000, 9000, and 11000, and zero-pressure gauge is used to apply to the pressure outlet condition. For helical coiled wire, stationary wall, negligible conduction heat transfer through the wire.

### 2.3 Numerical approaches, mesh Generation, and validation procedures

The Navier-Stokes and energy equations with boundary condition equations are solved using a computational fluid dynamics code (ANSYS FLUENT 22) based on finite volume methods. For pressure-velocity coupling, the SIMPLE method is employed, which is extensively utilized in numerical modeling of heat exchangers. By utilizing a link between velocity and pressure adjustments, this technique retrieves the pressure field while enforcing mass conservation. A second-order upwind technique was used to spatially discretize the momentum and energy equations, and a least squares cell-based gradient was employed. With a second-order spatial discretization of pressure, the velocity formulation was absolute. To attain second-order precision, the amounts of all cells were calculated using a multi-dimensional linear reconstruction technique. The governing equations with boundary conditions were solved using the pressure-based solver.

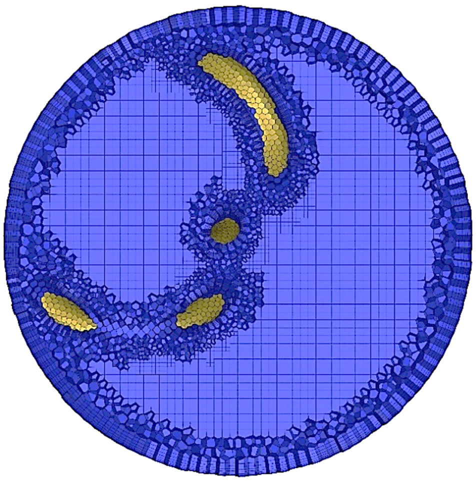

(a) Cross-section

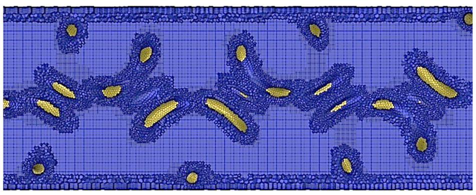

(b) longitudinal section

**Figure 4.** Generated mesh of hybrid elements (poly-hexacore) of tube fitted with CHCW.

**Table 2.** The studied cases and their specified grids.

| No. | Name | Grid elements |
|---|---|---|
| 1 | Plain tube | 0189,437 |
| 2 | CHCW − NT_1_7_10 | 5,605,757 |
| 3 | CHCW − NT_1.5_7_10 | 5,428,917 |
| 4 | CHCW − NT_2_7_10 | 5,314,945 |
| 5 | CHCW − TD_1_7_10 | 5,419,046 |
| 6 | THCW − NT_1_7_10 | 9,627,102 |
| 7 | THCW − NT_1.5_7_10 | 9,738,195 |
| 8 | THCW − NT_2_7_10 | 8,676,939 |
| 9 | THCW − TD_1_7_10 | 8,412,442 |

The initialization of the standard solution was calculated from the inlet. For continuity and velocities, the convergence requirement was ($1x10^{-5}$) for the absolute criteria of residual, while for energy, the highest value of the absolute criteria was ($1x10^{-6}$). In the context of simulation, mesh generation assumes a critical role, significantly influencing the precision and reliability of computational results. The process of spatial discretization within the computational domain commences with mesh construction, dividing the physical space into discrete parts or cells. This foundational step directly impacts the simulation's ability to study and depict underlying physical processes effectively. Beyond ensuring an accurate representation of domain geometry, a well-constructed mesh facilitates the application of governing equations and conservation laws. Consequently, simulations can precisely capture fine system characteristics and govern multiple spatial scales, all made possible by meticulously generated meshes [24]. In the present work, the 3D domains of studied cases were divided using hybrid mesh because of the complexity of these flow domains. The meshing steps in Workbench, ANSYS 22 by using Fluent With Fluent Meshing were utilized to get the meshes of the studied cases. The generated mesh for the studied case of tubes fitted with CHCW, are shown, in Fig. 4.

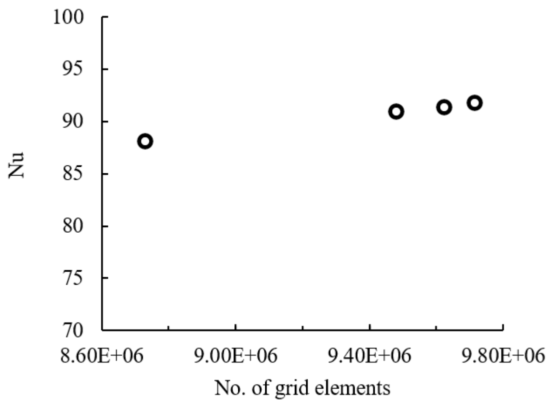


(a) Nusselt number

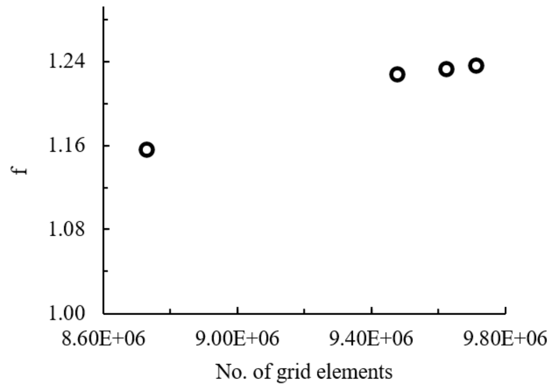


(b) Friction factor

**Figure 5.** Computed outcomes for a tube equipped with the THCWTD_1_7_10 configuration under varying grid densities at Re = 7000 for.

To confirm the grid independence of the performed numerical simulations, the grid refinement process was evaluated for each case under study by segmenting the domain into various grids and comparing the outcomes of the friction factor and Nusselt number. The associations between the friction factor, Nusselt number, and number of grid elements for the chosen case are shown in Fig. 5. As indicated in Fig. 5, the difference between the results obtained from successive grids diminishes with finer grids, reflecting the convergence of these results. In all the cases examined in this study, a deviation of less than 2% in both the friction factor and the Nusselt number is deemed acceptable for choosing a grid that will yield stable and grid-independent results. The reduction in deviation when using finer meshes is due to a decrease in the errors associated with applying the governing equations, which is a result of the reduced intervals of these equations' applications. Given the chosen constraint of a deviation in the results, the specific grid for each case is presented in Table 2. For each specified Reynolds number, the average computational cost for performing a simulation, except that for the plain tube, was typically between 4 and 5 hours. Given the lack of open-access researches on the use of helical coiled wire as an insert for enhancing thermo-hydraulic performance, it is necessary to conduct a validation study with typical triangular helical wires, as well as with plain tube.

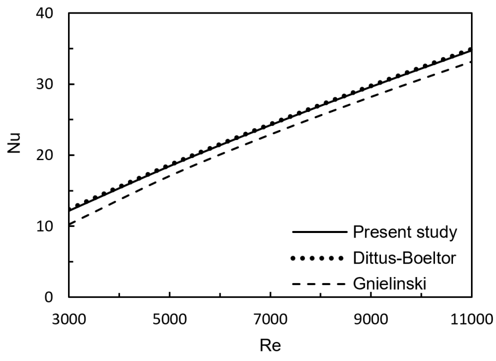


**Figure 6.** Nusselt number comparison for a plain tube.

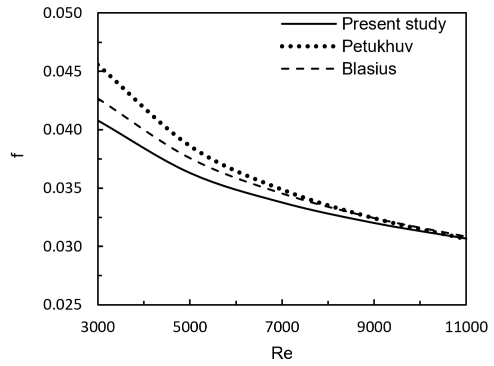


**Figure 7.** Friction factor comparison for plain tube.

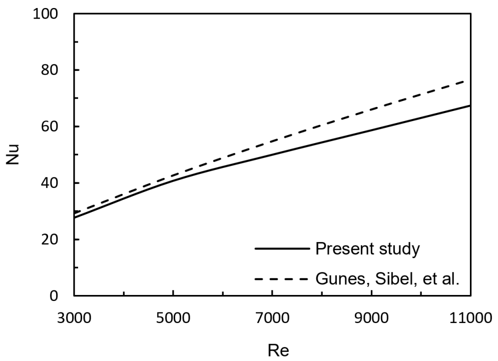


**Figure 8.** Nusselt number comparison for a plain tube equipped with a typical triangular helical wire.

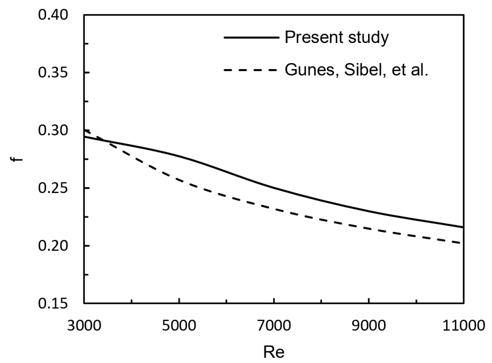


**Figure 9.** Friction factor comparison for plain tube equipped with a typical triangular helical wire.

Consequently, a new model of a typical triangular helical wire was developed. This model was designed to be consistent with the validated model and was tested under identical simulation conditions to those for the main models. The numerical outcomes for the Nusselt number and Darcy friction factor, both for a plain tube and tubes fitted with typical triangular helical wires, were compared with findings from studies [25]. This comparison was conducted to confirm the validity and acceptability of the results obtained in this work. The Nusselt numbers obtained from the plain tube were evaluated against the Gnielinski correlation [26]. For Reynolds numbers Re = 9000 and 11000, the Dittus-Boelter correlation [27] was used for comparison. The obtained friction factor results from the plain tube were compared with the correlations presented by Petukhov and Blasius [27]. The outcomes for the Nusselt number and friction factor, resulting from the tube equipped with a typical triangular helical wire in this study, were compared with the correlations found in the experimental research conducted by Gunes, Sibel, et al. [28]. As depicted in Fig. 6, the theoretical Nusselt number for the plain tube is validated. The numerical outcomes of the current study align with prior research, exhibiting an average deviation of 7.8% with the Gnielinski correlation along the whole Reynolds number range examined in this study. Furthermore, a minimal deviation of 0.7% was observed when compared with the Dittus-Boelter correlation for Reynolds numbers greater than or equal to 9,000. In Fig. 7, the validation of the theoretical friction factor results for the plain tube, as derived in the present study, is depicted. It is discernible that the numerical friction factor outcomes exhibit a noteworthy level of agreement with the prior investigations conducted by Petukhov and Blasius. The comparative analysis reveals that the average deviation amounts to 4.2% and 2.4%, respectively. Figure 8. validates the theoretical Nusselt number results derived in this study for a tube equipped with a typical triangular helical wire. The numerical outcomes were consisted with previous research, showed an average deviation of 8.4% when compared with the correlation from the study conducted by Gunes, Sibel, et al. Figure 9. provides validation for the theoretical friction factor results that were obtained in this study for a tube fitted with a typical triangular helical wire. The numerical outcomes demonstrated an average deviation of 5.9% when compared with the correlation from the study conducted by Gunes, Sibel, et al. It's important to highlight that the research carried out by Gunes, Sibel, et al., which was utilized for the last validation, had its findings corroborated by an additional experimental study conducted by Keklikcioglu, Orhan, et al [29].

## 3. Results and discussion

### 3.1 Velocity contours

The purpose of the current section is to meticulously analyze the physics governing the flow across the domain. The velocity vectors have been amalgamated with the streamwise velocity magnitude showed in velocity contours. For an airflow characterized by a Reynolds number $Re = 3000$, the results corresponding to axial locations of 0.150, 0.250, 0.350, and 0.450 $m$, measured from the tube inlet, depicted in frames (a to d), are elucidated in Fig. 10, sequenced from left to right, respectively. Attributable to the influence of viscosity, the flow velocity within the plain tube (PT) domain, delineated in part (A) of Fig. 10, escalated as it receded from the tube wall towards its center, culminating in its apex at the center. Concurrently, frames (b to d) of the identical segment exhibit a congruent pattern of velocity distribution, a consequence of their positioning within the fully developed flow region. Contrarily, frame (a) presents a different pattern, as a result of its location in the developing flow region. The velocity distribution resulting from the insertion of $CHCW - NT\_1\_7\_10$ is displayed in part (B) of Fig. 10. The introduction of the wire induces a swirl or secondary flow, disrupting the flow pattern observed in the plain tube. This leads to a more intricate velocity distribution, as shown by the contours. The presence of regions with higher velocity magnitudes is now distributed in the near-wall region, thereby disrupting parts of the boundary layer. Unlike the plain tube, the frames (a to d) of this part display different velocity patterns, which are a result of the absence of fully developed flow and the enhancement of flow mixing due to the swirling flow. Generally, the insertion of $CHCW - NT\_1\_7\_10$, and the resulting swirl flow, causes the flow to change the location and distribution of its maximum velocity from one section to another, thereby enhancing flow mixing. In the scenario where models $CHCW - NT\_1.5\_7\_10$ and $CHCW - NT\_2\_7\_10$ were inserted, where the wire is stretched due to an increase in pitch ratio (P/D), the formation of high-velocity spots is delayed compared to the previous case. This is shown in parts (C) and (D) of Fig. 10., where the high-velocity spots appear in frame (b) instead of frame (a) in the previous case. However, in the case of model $CHCW - NT\_2\_7\_10$, the high-velocity spots appear even later, in frame (c), in the downstream region. In the cases of insertion of the equilateral triangular cross-section wire, shown in parts (F), (G), (H), and (I), these models stand out prominently compared to their circular cross-section counterparts. The repositioning of high-velocity spots to areas near the wall and the intensity of mixing become apparent early in the areas where the flow initiates at frame (a), continuing until the final frame (d). Notably, the mixing intensity decreases with an increase in pitch ratio (P/D), reaching its lowest levels in the $THCW-NT\_2\_7\_10$ model with a pitch ratio of 2. The efficacy of this wire type can be attributed to the presence of sharp edges in the triangular section and the obstruction formed by each of the three sides, resembling the effect of one face of a twisted tape.

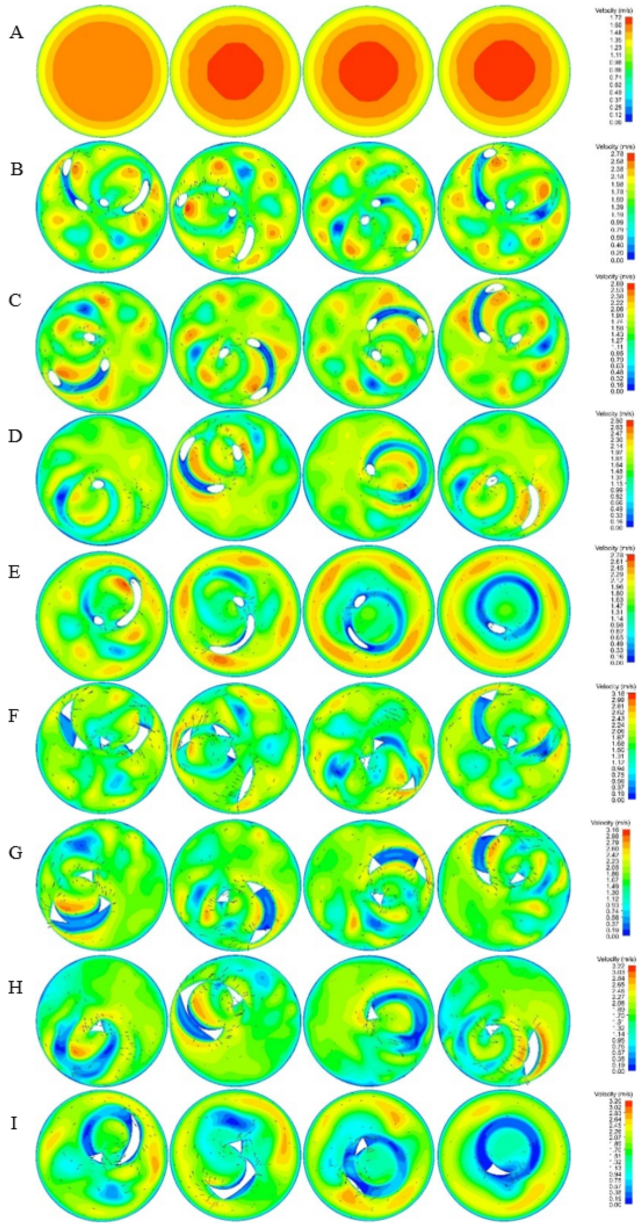


**Figure** 10**.** Velocity Contour overlaid with velocity vectors for PT (A), CHCW-NT_1_7_10 (B), CHCW-NT_1.5_7_10 (C), CHCW-NT_2_7_10 (D), CHCW-TD_1_7_10 (E), THCW-TD_1_7_10 (F), THCW-NT_1.5_7_10 (G), THCW-NT_2_7_10 (H), and THCW-TD_1_7_10 (I), for Re=3000 at axial locations from inlet (a) 0.150; (b) 0.250; (c) 0.350; and (d) 0.450 *m* arranged from left to right, respectively.

In a broader context, all studied models, characterized by a constant value of $R1 = 7$ *mm*, feature a helical coiled wire that prevents the formation of a hollow core along the axial centerline of flow. In other words, there is no continuous region in the fluid domain without blockage, except for that formed due to a clearance (S) of 1 *mm*, leading to flow disturbance in each section along the tube. This arrangement provides the advantage of optimal mixing.

## 3.2 Temperature contours

This section investigates the temperature variation across the domain. Figure 11. presented this variation in contour forms at axial locations of 0.150, 0.250, 0.350, and 0.450 *m*, measured from the tube inlet, as shown in frames (a to d) for airflow with $Re = 3000$. For plain tube (PT), part (A), the fluid temperature increases radially from the center to the tube wall in a circular pattern due to the absence of swirling flow. As the fluid flows more downstream from the first location of 0.150 *m* from the entrance, frame (a), to the locations of 0.250 and 0.350 m, frames (b and c), its temperatures increase forcing the colder region, which lies at the tube center, to be smaller and smaller due to increasing in heat absorbed by the fluid from the tube wall and the growth of thermal boundary layer.For the same reasons, frames (d and e) of this part showed that the temperature of the central region of flow increased continuously downstream.

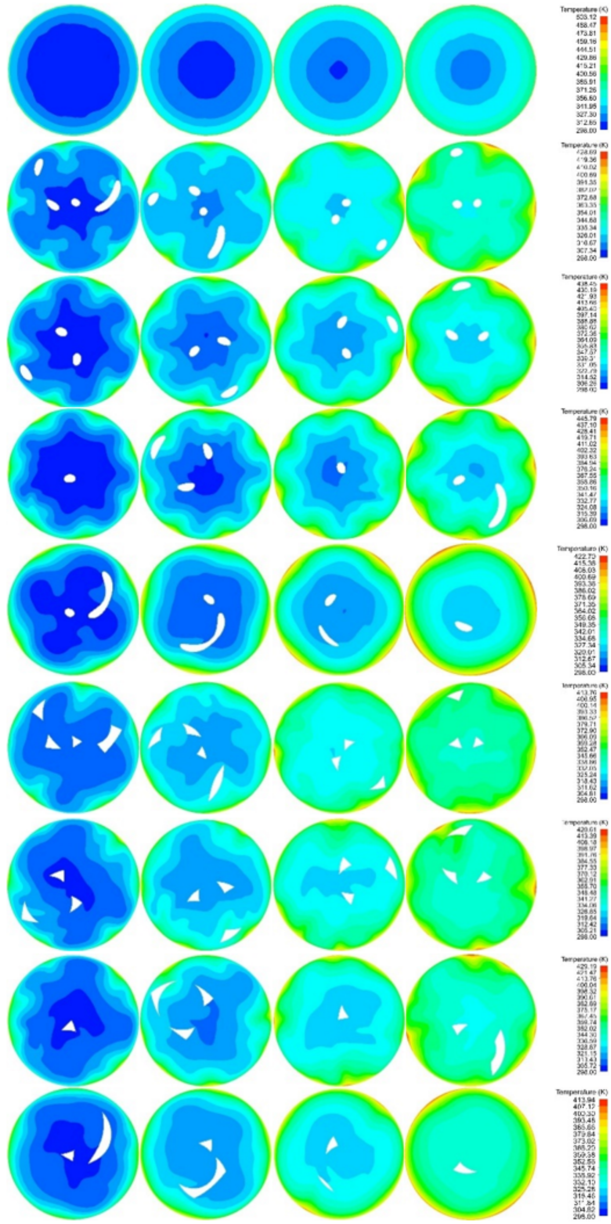

**Figure** 11**.** Temperature contour for; PT (A), CHCW-NT_1_7_10 (B), CHCW-NT_1.5_7_10 (C), CHCW-NT_2_7_10 (D), CHCW-TD_1_7_10 (E), THCW-TD_1_7_10 (F), THCW-NT_1.5_7_10 (G), THCW-NT_2_7_10 (H), and THCW-TD_1_7_10 (I), for Re=3000 at axial locations from inlet (a) 0.150; (b) 0.250; (c) 0.350; and (d) 0.450 *m* arranged from left to right, respectively.

The influence of the insertion of the $CHCW-NT\_1\_7\_10$, $CHCW-NT\_1.5\_7\_10$, and $CHCW-NT\_2\_7\_10$ models on the temperature distribution is demonstrated in Parts B, C, and D of Fig. 11, respectively. The incorporation of these models transforms the temperature distribution seen in the plain tube case into a star-shaped region, influenced by the wire's projection view along the flow direction, eliminating the circular pattern and pushing the colder region towards the tube wall due to the swirling flow. Similar to the PT, the fluid's high-temperature spots become largest as it travels further downstream inside the tube equipped with $CHCW-NT\_1\_7\_10$, as depicted in the frames of Part (B). A similar outcome can be observed for all cases, as shown in Parts (C to E) of the Fig. 11. Additionally, the insertion of HCW results in a significant increase in the area of hotter regions, attributable to enhanced flow mixing. In general, the use of HCW enhances the temperature distribution compared to the case of the plain tube. The pitch ratio (P/D) effect appears clearly when comparing the contours of the three models. The observation indicates that as the pitch ratio decreases, the fading of spots with lower temperatures initiates earlier in the upstream region of flow and vice versa. Model $CHCW-NT\_1\_7\_10$ here is the earliest in presenting this behavior, starting from frame (a), compared to the other two models in the same group. Regarding the equilateral triangular cross-section wire inserts, specifically models $THCW-NT\_1\_7\_10$, $THCW-NT\_1.5\_7\_10$, and $THCW-NT\_2\_7\_10$ shown in parts F, G, and H, respectively, these models, as in the case of velocity contours, stand out prominently compared to their circular cross-section counterparts. Fading of colder spots begins early in frame (b) in model $THCW-NT\_1\_7\_10$, compared to the case of model $CHCW-NT\_1\_7\_10$, where that happens later in frame (c). The shapes of the contours here are constantly distorted under the influence of the intensity of the disturbance arising from the pointed edges of the triangle's vertices. The repositioning of high-temperature spots to areas near the wall and the intensity of mixing become apparent early in the areas where the flow initiates at frame (a), continuing until the last frame (d). Notably, the intensity of redistributing decreases with an increase in pitch ratio (P/D), reaching its lowest levels in the $THCW-NT\_2\_7\_10$ model with a pitch ratio of 2, this phenomenon can be attributed to a reduction in the intensity of obstacles.

### 3.3 Nusselt number

The influence of utilizing a plain tube and the configurations of the studied cases on the average Nusselt number within turbulent airflow at various Reynolds numbers is elucidated in Fig. 12. As depicted in the illustration, the average Nusselt number exhibits an ascending trend with an increase in Reynolds number across all cases examined in the present work. This behavior can be attributed to the cumulative impact of heightened flow inertia forces arising from alterations in velocity and direction induced by the introduction of helical coiled wires. Furthermore, the figure underscores that the incorporation of any type of helical coiled wire model results in a higher Nusselt number compared to that of a plain tube. This enhancement is attributed to the generation of swirling flow patterns facilitated by the presence of the helical coiled wire inserts. The discernible rise in the Nusselt number signifies the augmented convective heat transfer efficiency associated with the implementation of helical coiled wire configurations within the studied Reynolds number range. It was observed that the equilateral triangular cross-section models significantly outperformed their circular cross-sectional counterparts, recording substantially higher Nusselt numbers. Fig. 13 depicts the Nusselt number ratio (Nu/Nup) results. As illustrated in the figure this ratio exhibits a decreasing trend with the increasing of the Reynolds number across all investigated scenarios. Notably, the Nusselt number results for $THCW-NT\_1\_7\_10$ demonstrate the most significant enhancement, reaching 4.14 to 3.6, followed closely by $THCW-NT\_1.5\_7\_10$ with a range of 3.95 to 3.6. Subsequent model $THCW-NT\_2\_7\_10$, 3.65 to 3.44.

### 3.4 Friction factor

While the presence of insertions can augment the Nusselt number, indicating enhanced heat transfer, it's important to note that this often comes with a trade-off in the form of an increased pressure drop. This increase is typically represented by the friction factor (f) [30]. Figure 14 illustrates the friction factor for turbulent airflow in both a plain tube and a tube equipped with the studded models at different Reynold numbers. The figure shows a decreasing trend in the friction factor as the Reynolds number increases in all the scenarios studied. This is due to the simultaneous increase in velocity that accompanies the rise in Reynolds number. Furthermore, the figure shows that the models $THCW-NT\_1\_7\_10$, $THCW-NT\_1.5\_7\_10$, and $THCW-NT\_2\_7\_10$ display higher friction factors compared to other models and the plain tube. This is due to the swirling flow and flow blockage caused by the sharp edge of the triangular shape, which is not present in the circular models, leading to a longer flow path. The increase in coil density resulted from low pitch ratio within the fluid domain also contributes to the increased blockage and extended flow path. Figure 15 shows the graphical representation of the friction factor ratio (f/fp) results against the Reynolds number. While models featuring a circular cross-section show a reduction in the friction factor ratio as the Reynolds number increases.

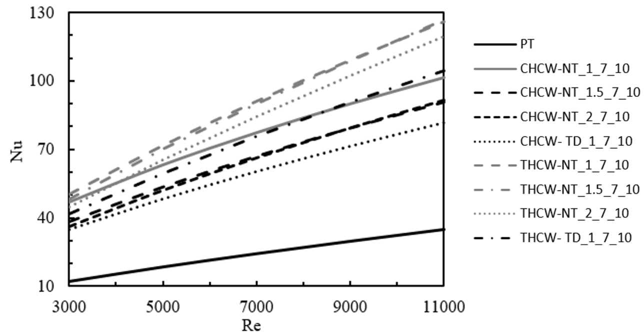


**Figure** 12**.** Average Nusselt number corresponding to a tube equipped with helical coiled wires, and plain tube.

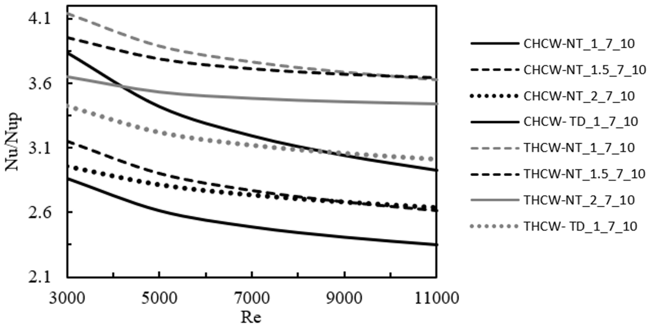


**Figure** 13**.** Nusselt number ratio corresponding to a tube equipped with helical coiled wires.

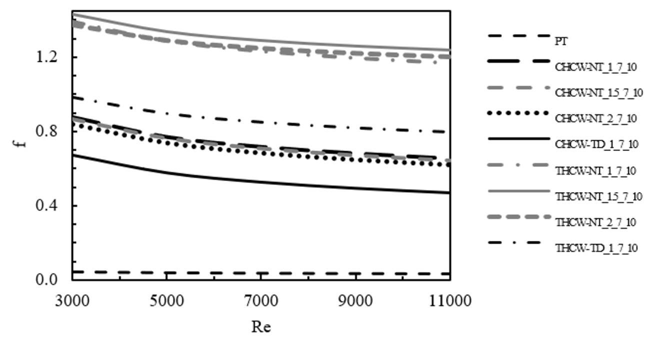


**Figure** 14**.** Friction factor corresponding to a tube equipped with helical coiled wires, and plain tube.

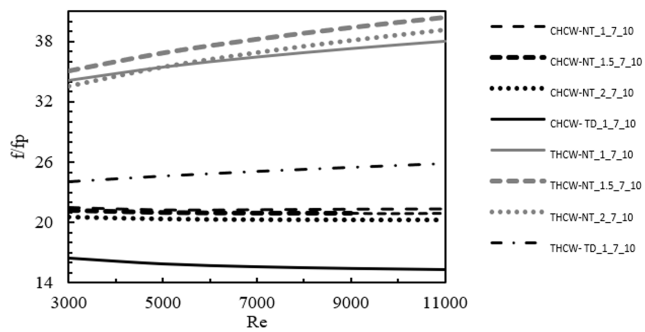


**Figure** 15**.** Friction factor ratio corresponding to a tube equipped with helical coiled wires.

Those with a triangular cross-section display an opposite behavior, with the friction factor ratio increasing alongside the Reynolds number, this pattern aligns with the findings presented by researcher comment [28] [31–35].

### 3.5 Thermal performance factor (TPF)

The thermal performance factor (TPF) stands as a pivotal parameter in the assessment of heat transfer enhancement techniques, such as the utilization of helical coiled wire inserts within tubes. It offers a comprehensive metric by integrating both the augmentation in heat transfer and the corresponding rise in pressure drop attributable to the presence of inserts. This factor was computed utilizing Eq. 6, proposed by Webb [36].

$$TPF = (Nu/Nu_p)\,/\,(f/f_p)^{-1/3} \tag{6}$$

In the context of the present investigation, an analysis of the TPF across various configurations and parameters becomes indispensable. By scrutinizing changes in coil geometry, configurations, and pitch ratios, insights can be gleaned into how these variables influence heat transfer enhancement, while aware of the associated alterations in pressure drop. The relationship between the TPF and the Reynolds number for the studied scenarios is graphically represented in Fig. 16. This graphical representation clearly indicates an inverse relationship between the Reynolds number and the TPF, i.e., an increase in the Reynolds number results in a decrease in the TPF. Among the various models studied, the model designated as $CHCW-NT\_1\_7\_10$, characterized by a P/D ratio of 1, R1 of 7 $mm$, and p of 10 $mm$, demonstrated a superior thermal performance factor specifically at Reynolds numbers of 3000, 5000, and 7000. While the model $THCW-NT\_1\_7\_10$ exhibited higher TPF values at Reynolds numbers of 9000 and 11000. The TPF values for the $CHCW-NT\_1\_7\_10$ model ranged from 1.379 to 1.053. Following was the model $THCW-NT\_1\_7\_10$, with TPF values ranging from 1.277 to 1.079, and model $THCW-NT\_1.5\_7\_10$, with TPF values ranging from 1.208 to 1.062. The models $THCW-TD\_1\_7\_10$, $THCW-NT\_2\_7\_10$, and $CHCW-NT\_1.5\_7\_10$ had TPF values ranging from 1.186 to 1.01, 1.132 to 1.01, and 1.138 to 0.94, respectively.

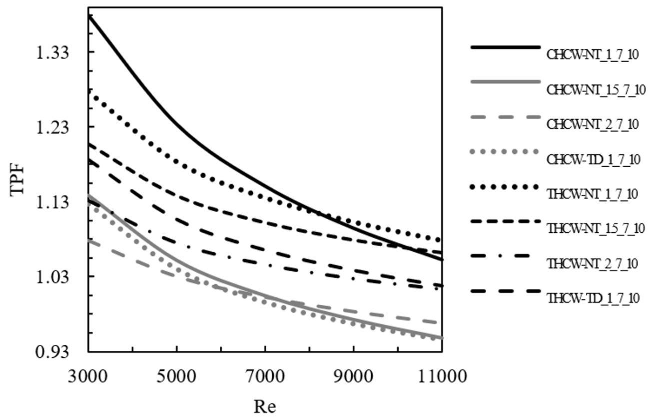


**Figure** 16**.** Thermal performance factor corresponding to a tube equipped with helical coiled wires.

## 4. Conclusions

The numerical investigation conducted in the present study focuses on the utilization of HCWs as turbulence and heat transfer promoters, aiming to elucidate their impact on both thermal and hydro-dynamic fields. Based on the results obtained, it can be deduced that the Nusselt number ratio and thermal performance factor both show a decrease as the Reynolds number increases. This trend is also observed in the friction factor ratio results for models with a circular cross-section. However, models with an equilateral triangular cross-section deviate from this trend, displaying a slight increase instead. An observable relationship emerges when considering the impact of variations in the pitch ratio (P/D) on the thermal performance factor, specifically, as the pitch ratio undergoes a reduction, there is a discernible trend characterized by a concomitant increase in the thermal performance factor. At a pitch ratio of (P/D) = 1, large base radius $R1 = 7$ $mm$, coiled wire pitch $p = 10$ $mm$, and $Re = 3000$, the helical coiled wire with both equilateral triangular and circular cross-sections achieved the maximum thermal performance factor of 1.379 and 1.277, respectively. Additionally, at the same parameters, the helical coiled wire with equilateral triangular cross-sections achieved the highest augmentation in the Nusselt number, with a Nusselt number ratio of 4.14. At $P/D = 1.5$, $R1 = 7$ $mm$, $p = 10$ $mm$, and $Re = 11000$, the helical coiled wire with equilateral triangular cross-sections achieved the highest increase in friction factor, with a friction factor ratio of 40.44.

## Authors' contribution

All authors contributed equally to the preparation of this article.

## Declaration of competing interest

The authors declare no conflicts of interest.


## Funding source

This study didn't receive any specific funds.


## Data availability

The data that support the findings of this study are available from the corresponding author upon reasonable request.


## Acknowledgements

The authors would like to acknowledge.


## REFERENCES


[1] L. Wang and X.-R. Zhang, "Industrial cooling systems, co2 refrigeration cycle and systems," *Cham: Springer International Publishing*, vol. 6, no. 12, pp. 313–336, February 2023. [Online]. Available: https://doi.org/10.1007/978-3-031-22512-3_10

[2] A. P. K. Dhumal, Amol R. and N. H. Ambhore, "A comprehensive review on thermal management of electronic devices," *Journal of Engineering and Applied Science*, vol. 70, no. 1, pp. 1–18, 2023. [Online]. Available: https://doi.org/10.1186/s44147-023-00309-2

[3] M. A. Oehlschlaeger, "Grand challenges in aerospace propulsion," *Frontiers in Aerospace Engineering*, vol. 1, no. 2022, p. 1027943, 2022. [Online]. Available: https://doi.org/10.3389/fpace.2022.1027943

[4] B. Bochenek and Z. Ustrnul, "Machine learning in weather prediction and climate analyses—applications and perspectives," *Atmosphere*, vol. 13, no. 2, p. 180, 2022. [Online]. Available: https://doi.org/10.3390/atmos13020180

[5] G. F. SMAISIM, "Augentation of heat transfer in corrugated tube using four -start spiral wall," *Al-Qadisiyah Journal for Engineering Sciences*, vol. 10, no. 4, pp. 451–487, 2017. [Online]. Available: https://search.emarefa.net/detail/BIM-839966

[6] S. H. Hussain], "Numerical investigation of the enhanced heat transfer due to curvature–induced lateral vortices in laminar flows over sinusoidal corrugated-plate channels," *Al-Qadisiyah Journal for Engineering Sciences*, vol. 2, no. 2, pp. 394–412, 2009. [Online]. Available: https://www.ncbi.nlm.nih.gov/books/NBK590948

[7] e. a. García, A., "The influence of artificial roughness shape on heat transfer enhancement corrugated tubes, dimpled tubes, and wire coils," *Applied Thermal Engineering*, vol. 35, no. 6, pp. 196–201, 2012. [Online]. Available: https://doi.org/10.1016/j.applthermaleng.2011.10.030

[8] J. Y. G. Chang, Shyy Woei and H. L. Shih, "Thermal performances of turbulent tubular flows enhanced by ribbed and grooved wire coils," *International Journal of Heat and Mass Transfer*, vol. 90, no. 2, pp. 1109–1124, 2015. [Online]. Available: https://doi.org/10.1016/j.ijheatmasstransfer.2015.07.070

[9] W.-C. H. San, Jung-Yang and C.-A. Chen, "Experimental investigation on heat transfer and fluid friction correlations for circular tubes with coiled-wire inserts," *International communications in Heat and Mass transfer*, vol. 65, no. 2, pp. 8–14, 2015. [Online]. Available: https://doi.org/10.1016/j.icheatmasstransfer.2015.04.008

[10] e. a. Sharafeldeen, M. A., "Experimental investigation of heat transfer and pressure drop of turbulent flow inside tube with inserted helical coils," *Heat and Mass Transfer*, vol. 53, no. 4, pp. 1265–1276, 2017. [Online]. Available: https://doi.org/10.1007/s00231-016-1897-z

[11] e. a. Du, Juan, "Experimental thermal and flow characteristics in a traverse corrugated tube fitted with regularly spaced modified wire coils," *International Journal of Thermal Sciences*, vol. 133, no. 1, pp. 330–340, 2018. [Online]. Available: https://doi.org/10.1016/j.ijthermalsci.2018.05.032

[12] e. a. Zimparov, Ventsislav, "Benefits from the use of wire-coil inserts in water transitional and low turbulent flow. the influence of the wire-coil pitch," *Thermal Science*, vol. 6, no. 7, pp. 60–60, 2022. [Online]. Available: https://doi.org/10.2298/TSCI211206060Z

[13] S. P. Hinge and A. W. Patwardhan, “Thermal-hydraulic performance of an annular pipe with square wire coil inserts using computational fluid dynamics,” *Industrial Engineering Chemistry Research*, vol. 59, no. 9, pp. 3887–3903, 2019. [Online]. Available: https://doi.org/10.1021/acs.iecr.9b04192

[14] H. Z. Y. W. M. Z. B. G. Yu, Chulin, “Numerical study on turbulent heat transfer performance of twisted oval tube with different cross sectioned wire coil,” *Case Studies in Thermal Engineering*, vol. 22, no. 5, p. 100759, 2020. [Online]. Available: https://doi.org/10.1016/j.csite.2020.100759

[15] M. R. A. H. M. A. G. M. H. A. H. Y. Khashayar Sharifi, Morteza Sabeti, “A good contribution of computational fluid dynamics (cfd) and ga-ann methods to find the best type of helical wire inserted tube in heat exchangers,” *International Journal of Thermal Sciences*, vol. 154, no. 54, p. 106398, 2020. [Online]. Available: https://doi.org/10.1016/j.ijthermalsci.2020.106398

[16] M. L. Y. Z. J. C. Yang, Yang, “Numerical study on heat transfer characteristics of molten salt in annular channel with wire coil,” *Applied Thermal Engineering*, vol. 199, no. 1, p. 117520, 2021. [Online]. Available: https://doi.org/10.1016/j.applthermaleng.2021.117520

[17] T. T. GÖKSU and F. YILMAZ, “Numerical comparison study on heat transfer enhancement of different cross-section wire coils insert with varying pitches in a duct,” *Journal of Thermal Engineering*, vol. 7, no. 7, pp. 1683–1693, 2021. [Online]. Available: https://doi.org/10.18186/thermal.1025930

[18] W. Dang and L.-B. Wang, “Convective heat transfer enhancement mechanisms in circular tube inserted with a type of twined coil,” *International Journal of Heat and Mass Transfer*, vol. 169, p. 120960, 2021. [Online]. Available: https://doi.org/10.1016/j.ijheatmasstransfer.2021.120960

[19] F. Aldawi, “Novel validated numerical analysis of flat coil tube with spring inserts,” *Case Studies in Thermal Engineering*, vol. 36, no. 4, p. 102197, 2022. [Online]. Available: https://doi.org/10.1016/j.csite.2022.102197

[20] R. H.-M. J. P.-G. J. S. García, A., “Validation of a new methodological approach for the selection of wire-coil inserts in thermal equipment,” *Applied Thermal Engineering*, vol. 218, p. 119273, 2023. [Online]. Available: https://doi.org/10.1016/j.applthermaleng.2022.119273

[21] P. C. Kumar, Rajan and H. Singh., “Experimental analysis of heat transfer in a triple tube heat exchanger with spring turbulator using cuo/water nanofluid,” *Journal of Nanofluids*, vol. 12, no. 2, pp. 429–437, 2018. [Online]. Available: https://doi.org/10.1166/jon.2023.1936

[22] e. a. Yin, Peng, “Evaluation of efficiency, thermohydraulic performance evaluation criterion, and field synergy principle improvement of the parabolic solar collector containing the hybrid nanofluid using spring turbulators,” *Case Studies in Thermal Engineering*, vol. 41, p. 102571, 2023. [Online]. Available: https://doi.org/10.1016/j.csite.2022.102571

[23] V. O. Keklikcioglu, Orhan, “Heat transfer augmentation in a tube with conical wire coils using a mixture of ethylene glycol/water as a fluid,” *International Journal of Thermal Sciences*, vol. 171, no. 1, p. 107204, 2022. [Online]. Available: https://doi.org/10.1016/j.ijthermalsci.2021.107204

[24] D. R. H. M. S. K. M. F. Yousif, “Numerical study of effect porous media on heat transfer in a horizontal annular tube,” *Al-Qadisiyah Journal for Engineering Sciences*, vol. 16, no. 4, pp. 289–297, 2023. [Online]. Available: https://doi.org/10.30772/qjes.2023.143069.1028

[25] D. N. A. zaid; Dhafer A Hamzah, “Heat transfer enhancement by turbulence generator inside heat receiver,” *Al-Qadisiyah Journal for Engineering Sciences*, vol. 13, no. 4, pp. 268–273, 2021. [Online]. Available: https://doi.org/10.30772/qjes.v13i4.680

[26] K. P. Dostál, Martin and S. Solnař, “Gnielinski’s correlation and a modern temperature-oscillation method for measuring heat transfer coefficients,” *EPJ Web of Conferences. EDP Sciences*, vol. 269, no. 01009, pp. 301–313, 2022. [Online]. Available: https://doi.org/10.1051/epjconf/202226901009

[27] D. Taler, “Simple power-type heat transfer correlations for turbulent pipe flow in tubes,” *Journal of Thermal Science*, vol. 26, no. 1, pp. 339–348, 2017. [Online]. Available: https://doi.org/10.1007/s11630-017-0947-2

[28] V. O. Gunes, Sibel and O. Buyukalaca, “Heat transfer enhancement in a tube with equilateral triangle cross sectioned coiled wire inserts,” *Experimental Thermal and Fluid Science*, vol. 34, no. 6, pp. 684–691, 2010. [Online]. Available: https://doi.org/10.1016/j.expthermflusci.2009.12.010

[29] O. Keklikcioglu and V. Ozceyhan, “Experimental investigation on heat transfer enhancement in a circular tube with equilateral triangle cross sectioned coiled-wire inserts,” *Applied Thermal Engineering*, vol. 131, no. 1, pp. 686–695, 2018. [Online]. Available: https://doi.org/10.1016/j.applthermaleng.2017.12.051

[30] M. G. Jehad, “Experimental study of the friction factor in equilateral triangular duct with different types of vorex generators (obstacles),” *Al-Qadisiyah Journal for Engineering Sciences*, vol. 3, no. 2, pp. 161–172, 2010.

[31] P. G. V. Garcia, Alberto and A. Viedma, “Experimental study of heat transfer enhancement with wire coil inserts in laminar-transition-turbulent regimes at different prandtl numbers,” *International journal of heat and mass transfer*, vol. 48, no. 21-22, pp. 4640–4651, 2005. [Online]. Available: https://doi.org/10.1016/j.ijheatmasstransfer.2005.04.024

[32] P. Promvonge, “Thermal performance in circular tube fitted with coiled square wires,” *Energy Conversion and Management*, vol. 49, no. 5, pp. 980–987, 2008. [Online]. Available: https://doi.org/10.1016/j.enconman.2007.10.005

[33] ——, “Thermal enhancement in a round tube with snail entry and coiled-wire inserts,” *International Communications in Heat and Mass Transfer*, vol. 35, no. 5, pp. 623–629, 2008. [Online]. Available: https://doi.org/10.1016/j.icheatmasstransfer.2007.11.003

[34] J. S. A. V. Martínez, D. S., “Heat transfer enhancement of laminar and transitional newtonian and non-newtonian flows in tubes with wire coil inserts,” *International Journal of Heat and Mass Transfer*, vol. 76, no. 2, pp. 540–548, 2014. [Online]. Available: https://doi.org/10.1016/j.ijheatmasstransfer.2014.04.060

[35] J. D. S. W. S.-M. H. W.-B. Y. Hong, Yuxiang, “Heat transfer and fluid flow behaviors in a tube with modified wire coils,” *International Journal of Heat and Mass Transfer*, vol. 124, no. 3, pp. 1347–1360, 2018. [Online]. Available: https://doi.org/10.1016/j.ijheatmasstransfer.2018.04.017

[36] R. Webb., “Performance evaluation criteria for use of enhanced heat transfer surfaces in heat exchanger design,” *Int. J. Heat Mass Transfer*, vol. 24, no. 4, pp. 715–726, 1981. [Online]. Available: https://doi.org/10.1016/0017-9310(81)90015-6


**How to cite this article:**
Murtadha A. Hanoon, Mohsen H. Fagr, and Kamaal S. Mekki. (2025). 'Flow and heat transfer augmentation using helical coiled wire of different cross-sections', Al-Qadisiyah Journal for Engineering Sciences, 18(2), pp. 202-210. https://doi.org/10.30772/qjes.2024.145936.1081